Thirupathi Sirisilla[1],
B. Mohan Naik[2]
P. Samir Chandra[3],
V. Madhu Kumar[4],
E. Krushi[5]

Step-Up Series Resonant DC–DC Converter with Bidirectional-Switch-Based Boost Rectifier for Wide Input Voltage Range Photovoltaic Applications

Journal of Electrical Systems

ABSTRACT: In order to facilitate photovoltaic (PV) applications, this research suggests a series resonant converter (SRC) based high gain DC-DC converter. In order to keep converter realization costs down, low-power applications often have a modest resonant inductance, leading to low-quality factor values; this research takes this into account. The switching frequency of these SRCs, however, is set. To control the input voltage across a broad range, the suggested architecture makes use of an alternating current (AC) switch. According to the results of this research, the current topology using a bidirectional switch can only regulate the input voltage within a certain range. To achieve circumvent this problem, the suggested converter rearranges the resonant tank so that is known as the capacitor that resonates located before to the bidirectional switch. The suggested converter has a lower duty cycle than its current equivalent at the same gain because the reorganization changes the dependency of the DC voltage gain on the duty cycle. A theoretical investigation reveals that, at maximum input current, the range for regulating we have an input voltage of expanded to include the area of large DC voltage gain values. In contrast to its predecessor, the suggested converter maintains its input voltage control range even when the resonant inductance values span a large range. Still, the suggested converter retains the SRC's benefits, namely the ability to flip on the primary-side semiconductor switches which use zero voltage switching (ZVS). At zero current, the output-side diodes are also disabled. We theoretically and experimentally compare the proposed converter to its current equivalent and its simulator. To back up the theoretical study of the suggested converter, a simulation is used.

Keywords: solar power, efficiency of conversion, bidirectional switch, series resonance converter, broad range converter, and direct current to direct current (DC-DC) converter.

1. INTRODUCTION

Transportation Electrification is seen as a practical way to move to renewable energy sources in light of the global warming that is becoming more apparent these days [1]. Power electronic converters are therefore confronted with a plethora of novel uses [2]. One growing need is for DC-DC converters that excel in performance that can accommodate DC microgrids that use minimal voltage power sources and battery storage [3]. For example, in power electronic applications involving photovoltaic (PV) modules, You must have the ability to regulate the input voltage range widely and perform high-voltage step-up in order to connect separate photovoltaic modules, which can produce the peak power they reach when drastically different voltages because of shading effects [4]. In order to extract the full power potential from a PV module, the DC-DC interface converter that goes along with it has to have excellent efficiency and a broad input voltage regulation range.

As a high-frequency transformer, galvanic isolation is often necessary applicable to applications requiring a step-up in voltage. The voltage variance has been addressed by several DC-DC converters [5-7]. A number of factors, including structure and complexity, distinguish these topologies. It was determined that the standalone buck-boost

[1]Assistant Professor, Department of Electrical and Electronics Engineering, Marri Laxman Reddy Institute of Technology and Management, Telangana, India.
2Assistant Professor, Department of Electrical and Electronics Engineering, Marri Laxman Reddy Institute of Technology and Management, Telangana, India
3B.Tech Student, Department of Electrical and Electronics Engineering, Marri Laxman Reddy Institute of Technology and Management, Telangana, India.
4B.Tech Student, Department of Electrical and Electronics Engineering, Marri Laxman Reddy Institute of Technology and Management, Telangana, India.
5B.Tech Student, Department of Electrical and Electronics Engineering, Marri Laxman Reddy Institute of Technology and Management, Telangana, India.

converters were the best option for wide-range, high-step-up applications. In order such that voltage buck and boost may be deployed features on separate converter sides, active switches are often located at both ends of the converter. Series resonant converters (SRCs) stand out among these topologies for their exceptional performance in certain PV applications. They allow the semiconductor components to soft-switch and make excellent use of the isolation transformer [8, 9].

Many industrial applications examine the LLC converter topology, which is comparable to the SRC architecture [10,11]. Although both converters use inductors, the SRC has a far larger ratio of magnetizing to resonant inductances than the LLC converter. To regulate the DC voltage gain, a resonant converter often makes use of frequency modulation. But tiny, inexpensive resonant inductors in the resonant tank are the focus of this research for low-power compact SRCs. The solution uses modification of pulse width (PWM) for controlling the DC voltage gain, which simplifies the converter design, but also leads to quality factor values that are poor. Typically, the front-end inverter of galvanically separated buck-boost SRCs uses pulse width modulation, pulse width modulation [12] or phase-shifted modulation [13] to perform the input voltage buck functionality. Countless investigations, some of which go back as 1988 [12], have already confirmed these modulation strategies. Recent research suggests that PSM and hybrid PSM approaches provide the best input voltage buck operating efficiency [14]. The implementation of the input voltage increase in the SRC is now receiving a lot of attention [8]. A boost rectifier is often used to do this [15]. Lessening the transformer turns ratio requires the boost rectifiers in this research are based on this rectifier that doubles voltage (VDR), which is designed for high-voltage step-up applications. Multiple pulses modulation [17] or short pulses [16] control the typical boost VDR's field-effect transistors based on metal oxide semiconductors, which are used to replace diodes. While switching out only one diode for a MOSFET might cut down on boost VDR power losses, doing so would increase the resonant inductor's peak current and perhaps lower its size [9].

However, switching losses may be greatly reduced by connecting an in-parallel four-way bidirectional switch with the transformer secondary winding, which alleviates the demand on the switch voltage. Concurrently, it maintains a constant balance between the resonant current's positive and negative magnitudes. This research takes into account the topology in [18] because of these benefits. Extensive testing has shown that this design is power and voltage inflexible. Hence, a different converter is suggested to rearrange a resonant reservoir parts' placements to increase the input voltage regulation range. Based on that architecture, the suggested converter layout shifts the resonance capacitor's location so that it lies between switching in both directions and the transformer's secondary winding [18]. In contrast to the baseline architecture from [18], the suggested converter is workable over a large variety of resonance inductance readings devoid of impacting the input voltage regulation range. A novel SRC architecture with a tweaked boost VDR is presented and tested in this work within the voltage range that is appropriate for PV module-level applications. Rearranging the location capacitor's resonant frequency may expand the power range and regulation voltage of the baseline architecture, according to the basic theory. We synthesized the ability to convert an enhanced control range for input voltage and power, identified and verified simulation- considerately, the boundaries while using the converter input voltage and power regulation range [18], and derived a simulation-verified steady-state mathematical model for the converter. Section 2 gives a detailed description of the suggested topology and an analysis of it, and the remainder of the work follows. In Section 3, we can see how the suggested SRC structure stacks up against the baseline. In Section 4, we go over the outcomes of the simulation verification. Section 5 concludes the whole thing.

2. TOPOLOGY AND MODULATION

2.1 Topology Description

Both the conventional and Figure displays the suggested topologies. 1ab. The proposed design makes advantage of the rectifier that doubles the voltage's output side. The proposed arrangement calls for the bidirectional switch to follow the resonance capacitor (Cr). At the same time, it is shown in Figure 1b as a crucial part of the rectifier that results in a voltage doubling. According to (1), a possible SRC design requires capacitors C1 and C2 with much higher capacitance than Cr in order to sustain a constant resonance frequency (fr). If an overflow inductance of the isolation transformer is modest, the resonance inductance Lr is equal to Llk. Otherwise, it is equal to the sum of Lext, the external inductance, and the leakage inductance of the transformer. If the transformer leakage is the only one used, the converter could be smaller and cheaper. For reasons that will become clear later on, the

resonant capacitor's average voltage (VCr) is zero because the VDR remains symmetrical throughout the switching period. As stated in the topology, the output voltage (VOUT/2) is half of the incorrect value for the average voltage across the resonant capacitors, denoted as Cr/2 [18]. An example of a bidirectional switch would be Q1 and Q2, two MOSFETs (metal-oxide-semiconductor field-effect transistors). To handle the input side, a standard voltage-source full-bridge inverter is used. Using complementary pulses with a duty cycle of about half, along with a little amount of dead time between control signals on the same leg, the transistors on the input side of the bridge are driven. The input voltage from the input-side full-bridge inverter is identical to the voltage with positive and negative magnitudes that the isolating transformer TX voltage receives when it receives a balanced rectangular signal. Both the main- transistors are able to switch more gently thanks to the supplementary circulating current provided by the transformer's magnetizing inductance (Lm). Their parasitic output capacitance may be recharged during the brief dead periods by means of the magnetizing current. The input bridge inverter supplies voltage to the isolating transformer TX, which increases it by a turn's ratio.

$$f_r = \frac{1}{2\pi\sqrt{L_r C_r}}$$

Lr stands for the resonant inductance.

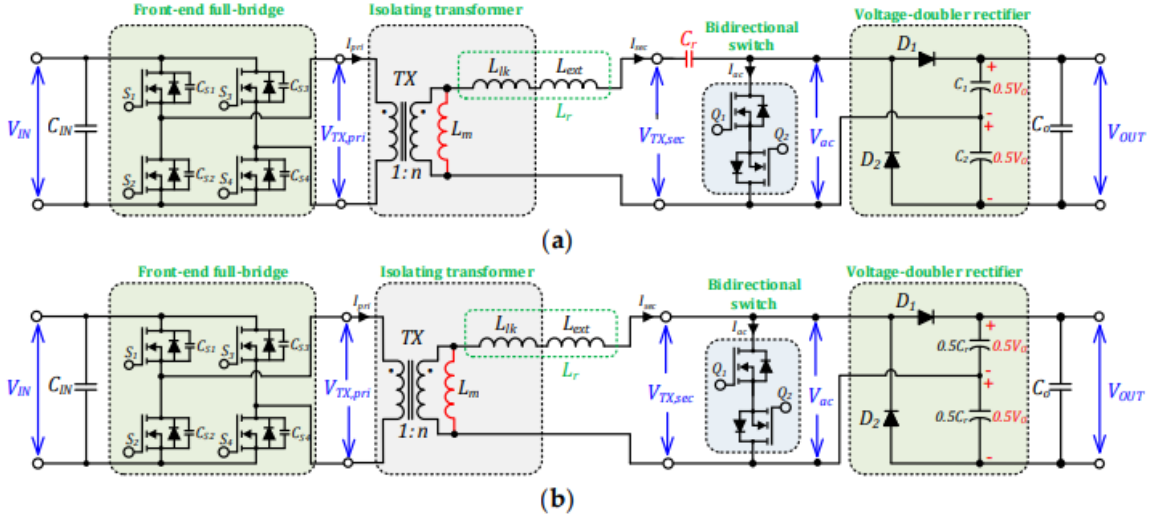

Figure 1. Both the SRC described in [18] and the one suggested here use a bidirectional switch in their converter topologies.

2.2 PWM Schemes for the Boost VDR

In a bidirectional switch, the two switches that make it up are Q1 and Q2. To increase the AC boost converter's efficiency, a resonant inductor is utilized to short-circuit the transformer's output winding. We set up a back-to-back arrangement of the two switches. The two-way switch may block both the positive and negative polarities of voltage and allows current to flow in either direction. Figure 2 shows two possible pulse width modulation (PWM) methods for generating the gating signal for switches Q1 and Q2. As seen in Figure 2a, the current initially passes through the other switch's body diode since only one switch is turned on per half-cycle. For example, in response to a positive half-wave across the transformer's secondary winding, transistor Q1 is turned on, which in turn forces transistor Q2's body diode to current.

The alternate pulse width modulation (PWM) technique shown in Figure 2b involves shifting the input-side switches' control signals such that they overlap with signals having an equal duty cycle, which in turn control the switches. Consequently, Reversal correction in real time is used to decrease conduction losses, and the body diodes are completely disregarded. As with the main-side switches, Q1 and Q2 have the same switching frequency in both scenarios. There are two equal periods During half the switching period TSW apart from the cumulative duty cycle Db, during which the voltage boosting mode occurs. Energy 2020, 13, x REVIEW BY FELLOW STUDENTS Fourteen out of fifteen are dual voltages.

The gate signal for the Q1 and Q2 switches might be generated using one of two pulse width modulation (PWM) techniques, as shown in Figure 2. Figure 2a shows that during each half-cycle, current flows through one switch's body diode because only one of the switches is switched on. For instance, when there is a positive the secondary winding in half-wave of the transformer, transistor Q1 is activated, which causes the body diode of transistor Q2 to current. The alternate pulse width modulation (PWM) technique shown in Figure 2b involves shifting the input-side switches' control signals such that they overlap with signals having an equal duty cycle, which in turn control the switches. Consequently, Reversal correction in real time is used to decrease conduction losses, and the body diodes are completely disregarded. As with the main-side switches, Q1 and Q2 have the same switching frequency in both scenarios. The voltage boosting mode is active for a total of two h-minute periods, each with its own cumulative duty cycle (Db).

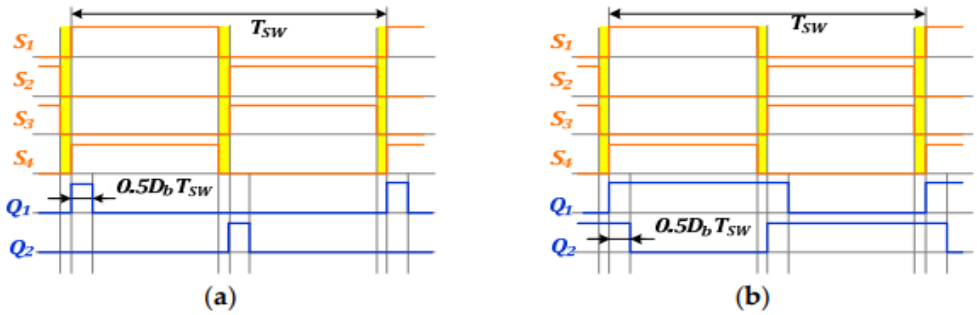

Figure 2: shows several PWM configurations for the bidirectional switch. Phase-shifted PWM with overlapping signals (b) and basic boost PWM (a) are the two types.

The suggested A increase to VDR for SRC operates abnormally in the PWM scheme shown in Figure 2b when ŸVCr/2 > nVIN, as shown in Figure 2. The bidirectional switch may use either a basic boost PWM or a phase-shifted PWM scheme with overlapping signals, as shown in Figure 2.

The output power level (POUT) affects the peak-to-peak ripple of the capacitor voltage, as stated in equation (2). It is worth mentioning that the proposed design can work with the PWM approach shown in Figure 2b, but only within a certain range of voltage and power. Any time the differential voltage between the capacitor's terminals (ΔVCr/2 > n·VIN) is higher than the maximum voltage that the transformer can handle, an irregular operation occurs. As seen in Figure 3, the current begins to flow in the opposite direction after the stored energy is discharged and a positive voltage is fed into the secondary winding of the transformer. This reverse current improves the system's efficiency and reduces the DC voltage gain by increasing the converter's conduction losses.

$$\Delta V_{Cr} = \frac{P_{OUT} T_{SW}}{2n V_{IN} C_r}$$

It is where VIN stands for input voltage, TSW for switching time, and n for transformer turns ratio.

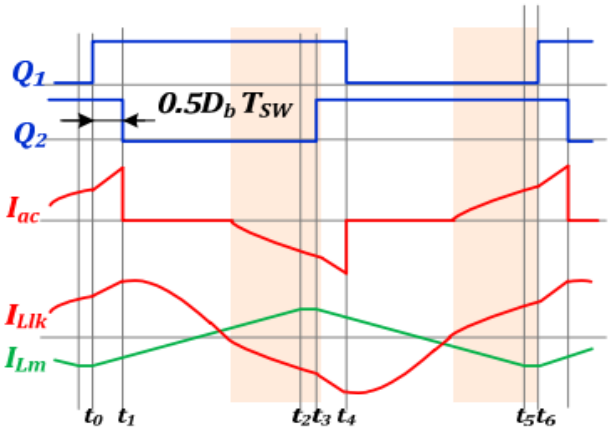

Figure 3 shows that while using PWM, the suggested SRC with a boost VDR operates abnormally.

3. Description of the Operating Principle

Both Figure 4 and Figure 5 show the main voltage and current waveforms, as well as the state-plane trajectory of the state variables, for the suggested design. The resonant current (iLlk(t)) is multiplied by the resonant impedance Zr, as indicated in (3), to provide the same axis units. In order to do the steady-state analysis, the following assumptions were made:

1. The output capacitance (CO) is large, therefore the output voltage (VOUT) is ripple-free.
2. The resonant capacitance (Cr) is much less than the output capacitances (C1, C2, CO).
3. Now, we'll apply the PWM method shown in Figure 2a to switches Q1, Q2.
4. No data is lost in the process.

The third The suggested converter's idealized steady-state voltage and current waveforms are shown in Figure 4. Figure 5 shows the planned SRC's resonance tank's state-plane trajectory. A1 A2 C2p The suggested converter's idealized steady-state voltage and current waveforms are shown in Figure 4. Shortcomings of conventional irrigation systems, while also integrating new elements to provide remote monitoring and encourage water efficiency. Improved agricultural yields, less water waste, and optimized irrigation systems are all possible thanks to this method. In order to overcome the drawbacks of conventional systems, the authors of the "IoT-Based Smart Irrigation and Controlling System" proposed the following innovations.

$$Z_r = \sqrt{\frac{L_{lk}}{C_r}}.$$

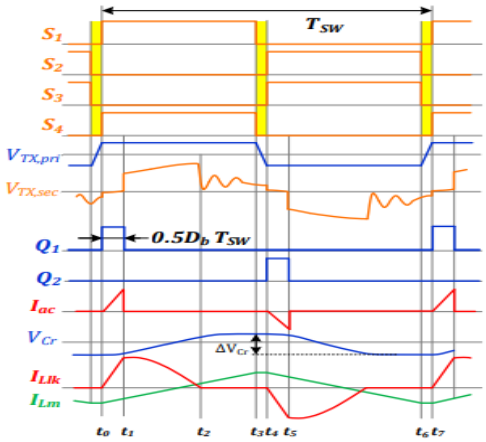

Figure 4. Drawn here are the idealized steady-state waveforms of the voltage and current for the suggested converter.

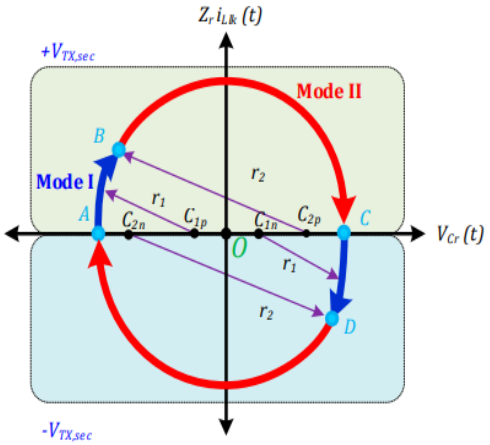

Figure 5. The state-plane trajectory of the resonance tank of the proposed SRC.

3.1 Modes of Operation

The first part of the voltage boosting mode, with a duty cycle of Db /2, is represented by Mode I, which has a time interval of [t0 < t ⊑ t1]. The primary winding of the transformer receives a positive voltage from the activated switches S1 and S4, whereas the secondary winding receives a voltage equal to nVIN. For your better understanding, Figure 6a displays the similar circuit of this interval. The resonance capacitor's voltage, -ΔVCr/2, is at its minimum at time t0. Switch Q1 will be turned on and the first resonance current will be almost zero when the conditions for nearly zero current switching (ZCS) are satisfied. The resonant capacitor's voltage and the secondary winding's voltage work together, similar to a conventional boost converter, to accelerate the charging of the resonant inductor. During this time, the voltage across the resonant capacitor moves from A to B on the state-plane in a fairly sinusoidal fashion, as seen in Figure 5. The variables representing the resonance current and voltage states are given by Equations (4) and (5), respectively, in the time domain.

The center of the trajectory arc segment is at (nVIN; 0), and the angular resonance frequency, denoted as ῠr = 2πfr, is in rad/s.

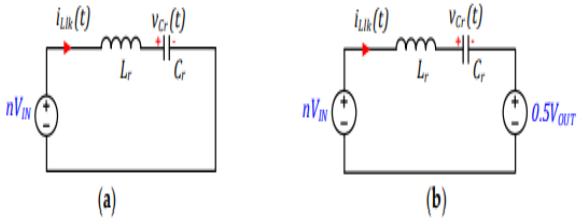

Intermediate node II: [t1 < t <= t2] The bidirectional switch current Iac goes to zero and the switch Q1 is turned off. See Figure 6b for an illustration of the direct release of energy from the resonant inductor to the load. In its forward-biased condition, diode D1 starts to conduct. At time t1, the resonant inductance current is equal to (VOUT/2 - nVIN), which is the same as the current but with the voltage polarity inverted. During this time, the voltage across the capacitor that resonates changes from point B to point C on the trajectory curve as the resonant inductor and capacitor resonate. This path's length is denoted from a certain vantage point β (in rad). At $\Delta X_{\circ}$□/2, the capacitor voltage is at its highest, and at t2, the resonant current is zero. Before the resonant current goes to zero, the converter operates in this mode, as described by Equations (7)–(9).

$$i_{Lik}(t) = \frac{r_2}{Z_r} sin(\beta - \omega_r(t - t_1)),$$

$$v_{Cr}(t) = nV_{IN} - \frac{V_{OUT}}{2} + r_2 cos(\beta - \omega_r(t - t_1)),$$

$$r_2 = -nV_{IN} + \frac{V_{OUT}}{2} + \frac{\Delta V_{Cr}}{2},$$

In this case, r2 is the radius of the section of the arc trajectory with its center at (0, (nVIN − VOUT/2);). Choice No. 3: from the interval [t2 < t ≤ t3] By turning off diode D1 at ZCS, all of the stored energy is released into the load in the prior mode, and the resonant current is zero. The converter goes into discontinuous conduction mode (DCM) when it stops delivering current to the load. The voltage across the capacitor stays at its peak at ΔVCr/2 until it reaches its termination at TSW/2 throughout this duration. At t3, the main switches (S1, S4) are turned off during the dead-time period (t3 < t <= t4), also called Mode IV. You may charge or discharge the parasitic output capacitance of switches (S2, S3) and (S1, S4) using the circulating current that goes to the main winding, accordingly. For this reason, prior to time instant t4, the connection between switches S2 and S3 is not voltage. Complete discharge of the parasitic capacitances in the switches requires that they achieve the values of the connected dead time and magnetizing inductance. Zero voltage switching (ZVS) allows the main switches to be switched on. The negative half-cycle of the switching period is represented by the time interval [t4 < t ⊑ t0] in Mode V. Throughout the time span [t0; t4], the converter maintains this condition.

3.3. DC Voltage Gain Derivation

The resonant tank's semi-circles, both positive and negative, are symmetrically represented by segments of the state-plane trajectory. Hence, the formula for the increase in DC voltage of the suggested converter is derived only from the trajectory segments A-B-C. Equations (10) and (11), correspondingly, provide a top-level equations for the circle radius in Mode I and Mode II, respectively. The intersection of the two circles at point B yields (12).

$$r_1^2 = (v_{Cr} - nV_{IN})^2 + (Z_r i_{Lik})^2,$$

$$r_2^2 = \left(v_{Cr} - nV_{IN} + \frac{V_{OUT}}{2}\right)^2 + (Z_r i_{Lik})^2,$$

$$(v_{Cr}(t_1) - nV_{IN})^2 + (Z_r i_{Lik}(t_1))^2 - r_1^2 = \left(v_{Cr}(t_1) - nV_{IN} + \frac{V_{OUT}}{2}\right)^2 + (Z_r i_{Lik}(t_1))^2 - r_2^2.$$

A value for voltage across the resonant capacitor and current via the resonant inductor at time t1 is given by:

$$i_{Lik}(t_1) = \frac{r_1}{Z_r} sin(\omega_r t_1),$$

$$v_{Cr}(t_1) = nV_{IN} + r_1 cos(\omega_r t_1)$$

The following is the process for deriving the resonance path angle β from Equations (7) and (13):

$$\beta = \pi - sin^{-1}\left(\frac{r_1}{r_2} sin(\omega_r t_1)\right).$$

Next, we may describe the converter's cumulative duty cycle as: by replacing t1 = DbTSW/2 in Equations (13)-(15):

$$D_b = \frac{2cos^{-1}\left(\frac{\frac{T_{SW} P_{OUT}}{4C_r}(4 - G_n) + nV_{IN}V_{OUT}}{nV_{IN}V_{OUT} + \frac{T_{SW} P_{OUT}}{4C_r} G_n}\right)}{\omega_r T_{SW}},$$

where the normalized DC voltage gain is denoted as Gn = VOUT nVIN. According to Equation (16), the duty cycle is affected by the resonance tank characteristics in addition to the converter output power level. Equation (17) gives the duty cycle Db for the topology in [18].

$$D_b = \frac{2L_{lk}\sqrt{\frac{2P_{OUT}T_{SW}}{V_{OUT}C_r}(V_{OUT} - nV_{IN})}}{Z_r n V_{IN} T_{SW}}.$$

3.4. Comparison of DC Voltage Gain and Input Operating Range

We evaluate the suggested topology in comparison to the standard [18] setup. An impressive aspect of the suggested layout is the input voltage regulation capability, which covers a broad spectrum of voltages and powers. By maintaining a constant duty cycle Db, the suggested converter outperforms the conventional SRC design in terms of DC voltage gain (Figure 7a). Also, unlike the standard SRC design, which uses the resonant inductance value to control the voltage and power regulation range, the suggested converter is far less sensitive to this value. According to Equation (16), the working range limit is shown in Figure 7b, with a maximum input voltage (VINm) of 30 V, an input current (IINm) of 20 A, and a maximum input power (PINm) of 300 W. We reduced the minimum input voltage to 10 V to keep the converter's power loss to a minimal. For PV module-level applications, the specified operating range is common; the interface converter has to work even while partially shaded, and the real maximum power point might happen at voltages as low as 10 V. Yellow highlights the spot where the fundamental SRC design from [18] doesn't work as expected, and it shows that Db = 0.8 is a major occurrence. Unlike Figure 7b, the simulated regulatory range of the basic design would be significantly constrained if the duty cycle value was always less than one (Db < 1).

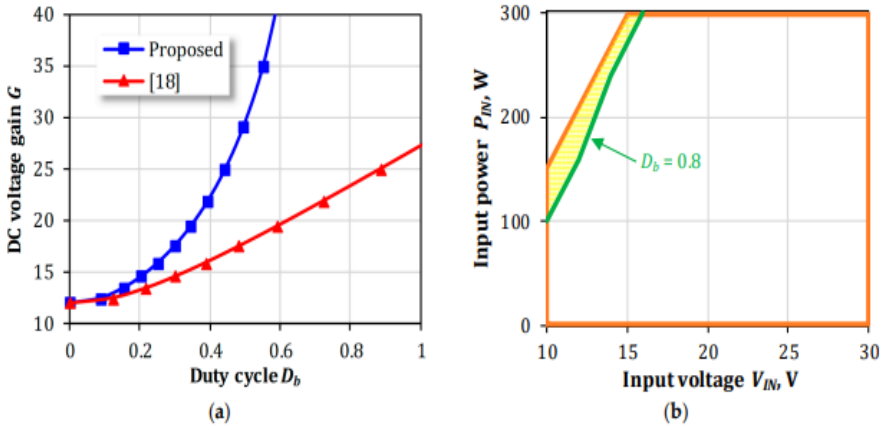

Figure 7. A comparison is made between the suggested layout and [18] with respect to (a) the DC voltage at PIN = 300 W and (b) the input voltage and power ranges for both the goal and achievable scenarios, with Lr = 100 H.

4. SIMULATION RESULTS

4.1. Description of the Simulation

Table 1. Setup parameters and components

Parameter	Symbol	Value
Input voltage range	V_{IN}	10:30 V
Input-side capacitor	C_{IN}	150 µF
Transformer leakage inductance	L_{lk}	4 µH
Transformer magnetizing inductance	L_m	1.3 mH
External inductor	L_{ext}	92.5 µH
Resonance capacitor	C_r	30 nF, metal film
Voltage-doubler capacitors	C_1, C_2	150 µF, electrolytic
Output-side capacitors	C_o	150 µF
Output voltage	V_{OUT}	350 V
Switching frequency	F_s	95 kHz
Components	**Symbol**	**Part Number**
Primary-side switches	S_1, S_2, S_3, S_4	FDMS86180
Bidirectional switch	Q_1, Q_2	SCT2120AF
Output-side diodes	D_1, D_2	C3D02060E

4.2. Steady-State Waveforms

Figure 8a-c shows the experimental waveforms of the proposed converter in steady state conditions with the maximum input voltage. It was decided to disable the bidirectional switch. and the operational power was set at 300W. Figure 8a shows that the square waveform for the transformer's primary winding voltage was produced by operating the primary switches S1, S2, S3, and S4 with an approximate duty cycle of 0.5. This converter was operating in DCX mode, which is a DC transformer. Under 10A of input current, the transformer primary recorded a peak-to-peak voltage of 60V. With a peak value of 8A, the main current displayed a periodic sine wave. Because of the parasitic capacitances in the semiconductors, voltage and current oscillations in the main winding were noted. Figure 8b shows a peak-to-peak voltage of 350V and a current of zero across the bidirectional switch. Similar to the main winding voltage, the secondary winding voltage followed a similar pattern, but with an n-fold increase in magnitude, reaching 180V. At 2.4A, the current through the secondary winding reached its maximum. There was a significant connection between the observed and theoretical height to height values of the resonance capacitor voltage, which were 175V and 174V, respectively, supporting the theoretical study. Capacitor C1 reflected half of the output voltage, or 175V, thus the voltage stayed steady at 350V. Although the predicted value of 280V was close, the actual voltage swing of the resonant capacitor was found to be 300V.

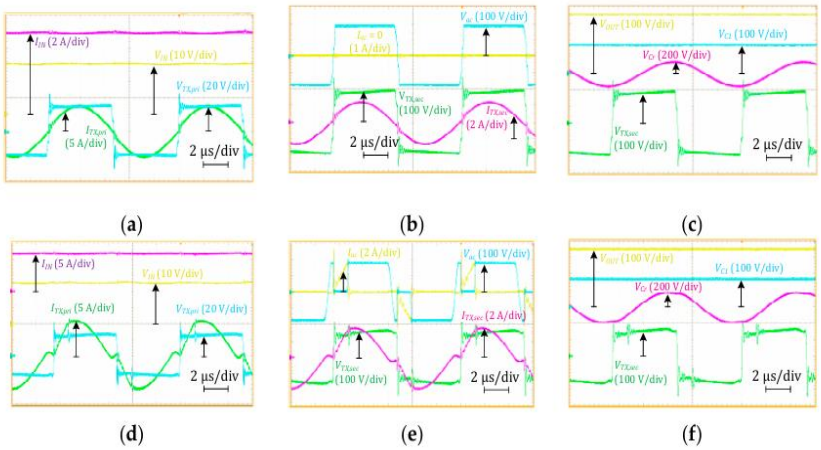

Figure 8 shows the experimental waveforms of the proposed converter in steady-state operation at different voltages and current densities: (a-c) 300 W PIN, 30 V VIN, and 0 Db; and (d-f) 300 W PIN, 25 V VIN, and 0.215 Db.

For the boost mode functioning of the converter, a current and voltage waveform at steady state are shown in Figure 8d-f. The input voltage was 25 volts and the working power was 300 watts. In the case of the bidirectional switch, the total duty cycle was Db= 0.215. Twelve amperes was the current taken from the power source. Roughly 230 V was the peak-to-peak ripple voltage, while the average voltage of the resonance capacitor was zero.

At VOUT = 350 V, the voltage at the output was steady. The output transistors' hard-switching caused small parasitic oscillations. The DCX mode causes the resonant tank's voltages and currents to be almost sinusoidal, which causes the state-plane trajectory to have a circular form. The resonant tank's voltages and currents are almost exactly sinusoidal, with the radius of each curve matching up to ΔX. All of the curves' radiuses are VCr-related.

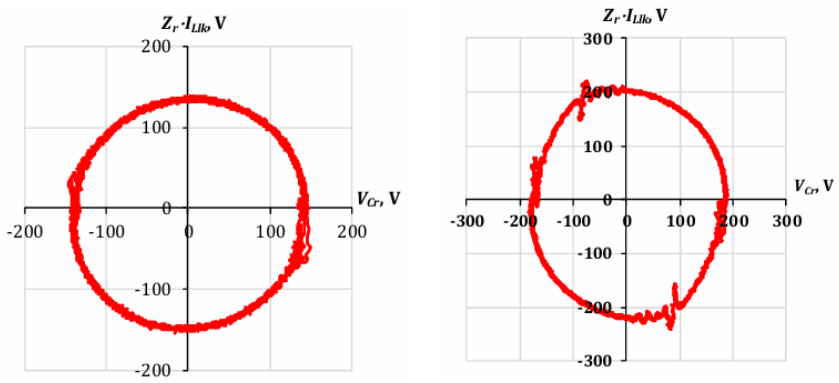

(a) (b)

Pictured in Figure 9 are the experimental state-plane trajectories of the DCX and boost modes, respectively, for the suggested converter operating at PIN = 300 W.

In Figure 10, the duty cycle is displayed against the converter's theoretical and actual conversion gains. When Db= 0 on the duty cycle, the converter's DC voltage gain is 12.0 volts. The minor discrepancies between the anticipated and actual DC voltage gain values are caused by power losses. The difference between the expected and measured DC voltage gain values becomes more noticeable when the input power is 200 W as the converter undergoes higher losses at this level. With 50 W PIN and a gain of 20 V, the duty cycle is Db = 0.22 and Db = 0.32, respectively, demonstrating that the duty cycle at a particular DC voltage gain changes with the input power level.

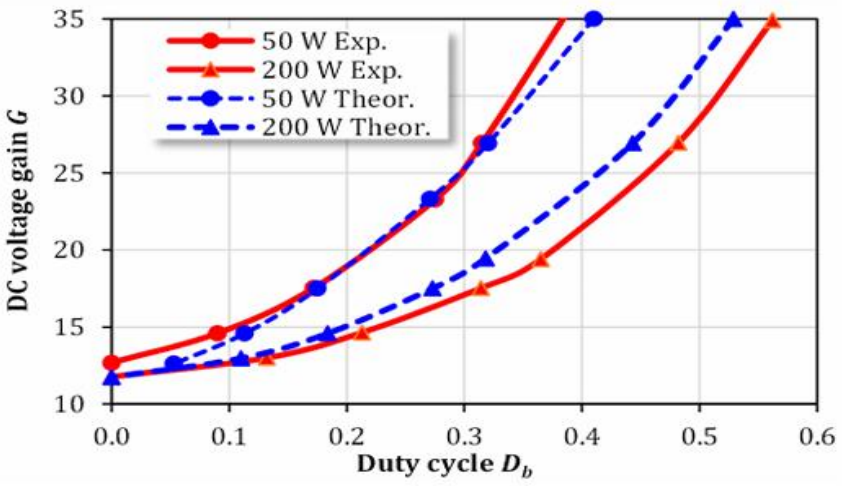

Figure 10 shows the DC voltage gain of the converter as a function of duty cycle and two different input power levels, as calculated and observed.

Both the baseline and the proposed topologies had their input voltage regulation ranges tested. Baseline converters from [18] have more limited input voltage and power regulation ranges than theoretical projections, which is not surprising. The recommended converter outperforms the baseline converter from [18] because its input voltage and power range is shorter than theoretical projections (as seen by the yellow-highlighted section of Figure 11). From what we can see in the experiments, this improves over the baseline converter from [18]. Experiment results show that the baseline converter loses control of the voltage at duty cycles exceeding a crucial threshold, which drops practically linearly from 0.7 at VIN = 10 V to 0.46 at VIN = 22 V; this limit is shown by the green line in Figure 11.

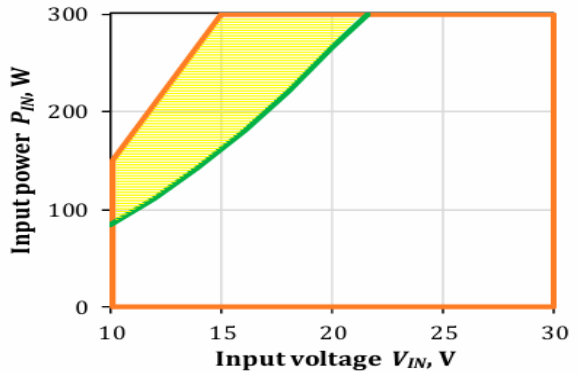

The experimental limit of the input voltage and power regulation range compared to the intended operating range for the proposed and baseline SRC topologies is shown in Figure 11.

After that, you must test the converter's efficiency using varying input voltages and power levels. Across a broad input voltage range, Figure 12a displays the observed efficiency. At PIN= 50 W and PIN= 200, the suggested converter achieved a maximum efficiency of 96% and 96.5%, respectively. At full input voltage (Db = 0), with the bidirectional switch set off, these values were obtained. There was a sinusoidal structure to the transformer current, and the converter was very much like a classic SRC. The converter semiconductors successfully underwent complete soft-switching as a result. The converter increased the transformer voltage to 350 V by activating pulse width modulation (PWM) of the bidirectional switch in response to a drop in the input voltage. When Db > 0, the converter's soft-switching functionality is disabled, resulting in reduced efficiency as the input voltage rises and increased conduction losses. The operating power also had an effect on efficiency as a result of the resonant tank's quality factor shift. Figure 12b shows the results of a comparison of input power and efficiency for a range of input voltages. When applied to input voltages greater than 20 V, the efficiency curves remain flat across the large input power range.

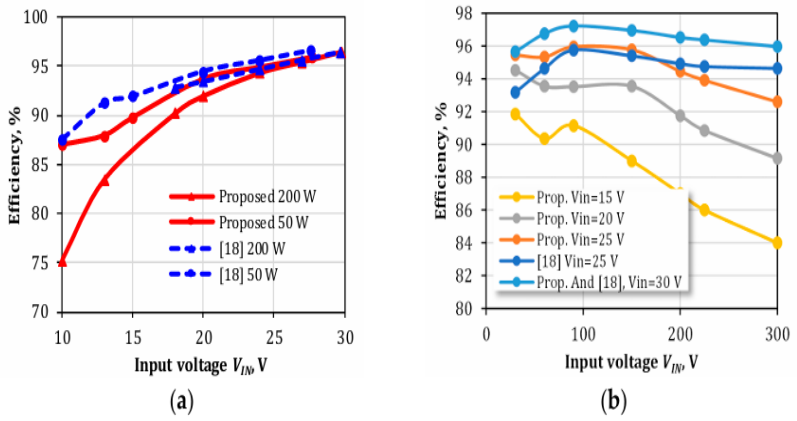

Figure 12 shows a comparison of the observed efficiency of the baseline converters and the suggested converters with respect to (a) the input voltage at two power levels and (b) the input power at various power levels.

A two-level input voltage and (b) a variety of input voltages and input powers. In order to compare the baseline converter from [18] with the proposed converter, Figure 12 additionally provides several efficiency curves for the baseline. It is worth mentioning that the converter being suggested has somewhat lower 4. Power-Efficient Experimental Results 4.1. Experimental Prototype Description, which is a consequence of the bidirectional switch's increased voltage stress Figure 12b shows that at an input voltage VIN = 25 V, the suggested design achieves greater efficiency under light loads. Nonetheless, given that the converter under consideration is capable of In order to compare the baseline converter from [18] with the proposed converter, Figure 12 additionally provides several efficiency curves for the baseline. Note that the suggested converter's efficiency drops somewhat with increasing power. This is because the bidirectional switch experiences more voltage stress while running at low input voltages and large input currents, two of the most important operating points (see Figure 11). Figure 12a shows that, for an input voltage lower than 18 V, the converter from [18] is unable to provide an input power greater than 200 W. To ensure the suggested converter could execute maximum power point tracking (MPPT), an application-specific analysis was carried out. Following the same logic as in [21], a streamlined control strategy was implemented using the hill-climbing MPPT algorithm in conjunction with direct duty cycle perturbations. while the duty cycle Db was raised, the input voltage for the supplied converter decreased while operating with a PV module. Therefore, a PI controller is unnecessary when using the direct MPPT. The test was conducted in constant voltage mode with the electronic DC load Chroma 63204 with the input power source being the solar array simulator (SAS) Agilent E4360A. Figure 13 shows the MPPT procedure that corresponds to the operation of the converter with a Sharp NQ-R258H 48-cell monocrystalline-Si PV module. The charging of the internal capacitances caused the current spike to arise when the converter was first connected to the SAS. The DC load began operating and the converter took the minimal current from the SAS required to maintain the DC load running as soon as the output voltage hit 350 V, the reference value. After then, the MPPT began after 0.6 seconds had passed. In 2.5 seconds, the converter achieved the maximum power point of the matching PV module. Notably, start-up transients led the resonant capacitor to encounter an o set of around 200 V. However, after a few seconds of use, this o set vanished. Most notably, the input power was clearly demonstrated to have a close relationship with the voltage ripple of the resonant capacitor.

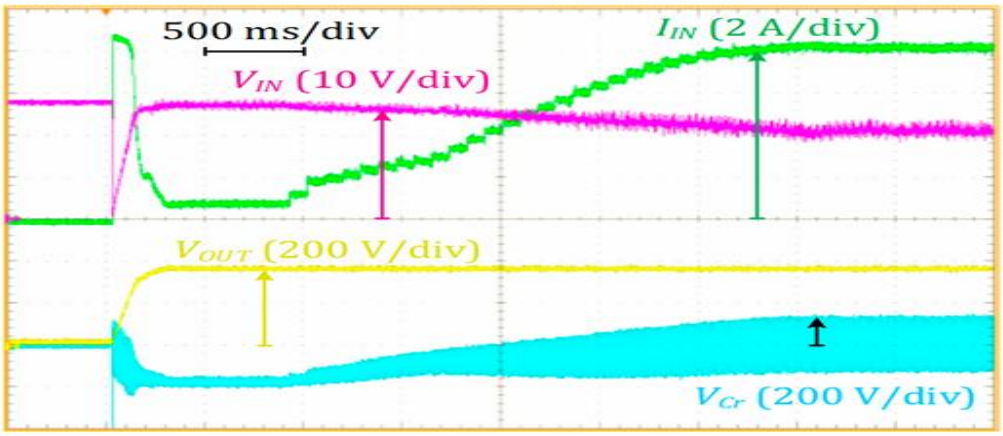

Figure 13. Experimental MPPT routine.

5.CONCLUSION

This research introduces a novel series resonant DC-DC converter with the ability to increase voltage via the boost voltage-doubler rectifier on the output side. In the suggested converter, the resonant capacitor is placed between the transformer's secondary winding and the bidirectional switch, which is different from the baseline design. If the fundamental design is not there, the suggested converter can nevertheless function over a wide range of low voltages and high currents. The efficiency of the suggested converter is compromised, however, since it is subjected to greater bidirectional switch voltage stress than its baseline counterpart because of the resonant capacitor voltage ripple. But even at its most efficient, the suggested converter uses the whole input voltage and power operational range, achieving 96.5%. With its broad voltage range of potential maximum power points that may be recognized during shadow operation and its ability to monitor the maximum power point, the suggested

converter was suitable for PV module applications. The suggested converter has a major design flaw with the isolating transformer that makes its implementation difficult. When money is tight, it's best to include the resonant inductor within the transformer. However, this approach comes with the risk of undesirable proximity losses in the transformer windings. As a result, improving the converter's passive components will be the primary emphasis of future studies. Critical Factors Section 3.2.1

6. REFERENCES

1. Dennis, K. Environmentally beneficial electrification: Electricity as the end-use option. Electr. J. 2015, 28, 100–112. [CrossRef]

2. Zhang, G.; Li, Z.; Zhang, B.; Halang, W.A. Power electronics converters: Past, present and future. Renew. Sustain. Energy Rev. 2018, 81, 2028–2044. [CrossRef]

3. Batarseh, I.; Alluhaybi, K. Emerging opportunities in distributed power electronics and battery integration: Setting the stage for an energy storage revolution. IEEE Power Electron. Mag. 2020, 7, 22–32. [CrossRef] Energies 2020, 13, 3747 14 of 14

4. Ravyts, S.; Van de Sande, W.; Vecchia, M.D.; den Broeck, G.V.; Duraij, M.; Martinez, W.; Daenen, M.; Driesen, J. Practical considerations for designing reliable DC/DC converters, applied to a BIPV case. Energies 2020, 13, 834. [CrossRef]

5. Cha, H.; Peng, F.Z.; Yoo, D. Z-Source resonant DC-DC converter for wide input voltage and load variation. In Proceedings of the 2010 International Power Electronics Conference—ECCE ASIA, Sapporo, Japan, 21–24 June 2010. [CrossRef].

6. LaBella, T.; York, B.; Hutchens, C.; Lai, J.-S. Dead time optimization through loss analysis of an active-clamp flyback converter utilizing gan devices. In Proceedings of the 2012 IEEE Energy Conversion Congress and Exposition (ECCE), Raleigh, NC, USA, 15–20 September 2012. [CrossRef]

7. Wang, Y.; Liu, R.; Han, F.; Yang, L.; Meng, Z. Soft-Switching DC–DC converter with controllable resonant tank featuring high efficiency and wide voltage gain range. IET Power Electron. 2020, 13, 495–504. [CrossRef]

8. Chub, A.; Vinnikov, D.; Lai, J.-S. Input voltage range extension methods in the series-resonant dc-dc converters. In Proceedings of the 15th Brazilian Power Electronics Conference and 5th IEEE Southern Power Electronics Conference (COBEP/SPEC'2019), Santos, Brazil, 1–4 December 2019. [CrossRef]

9. Kim, J.-W.; Park, M.-H.; Han, J.-K.; Lee, M.; Lai, J.-S. PWM resonant converter with asymmetric modulation for ZVS active voltage doubler rectifier and forced half resonance in PV application. IEEE Trans. Power Electron. 2020, 35, 508–521. [CrossRef]

10. Fei, C.; Lee, F.C.; Li, Q. High-Efficiency high-power-density LLC converter with an integrated planar matrix transformer for high-output current applications. IEEE Trans. Ind. Electron. 2017, 64, 9072–9082. [CrossRef].